Solution Processing of Hydrogen-Terminated Silicon Nanocrystal for Flexible Electronic Device

Kano, Shinya
Tada, Yasuhiro
Matsuda, Satoshi
Fujii, Minoru

(Citation)
ACS Applied Materials & Interfaces,10(24):20672-20678

(Issue Date)
2018-06-20

(Resource Type)
journal article

(Version)
Accepted Manuscript

Solution processing of hydrogen-terminated silicon nanocrystal for flexible electronic device

Shinya Kano, Yasuhiro Tada, Satoshi Matsuda, and Minoru Fujii*

Department of Electrical and Electronic Engineering, Graduate School of Engineering, Kobe University, Rokkodai, Nada, Kobe 657-8501, Japan

ABSTRACT

We demonstrate solution processing of hydrogen-terminated silicon nanocrystals (H-Si NC) for flexible electronic devices. To obtain high and uniform conductivity of a solution-processed Si NC film, we adopt a perfectly dispersed colloidal H-Si NC solution. We show a high conductivity (2×10^{-5} S/cm) of a solution-processed H-Si NC film which is spin-coated in air. The NC film (area: 100 mm^2) has uniform conductivity and responds to laser irradiation with 6.8 and 24.1 μs of rise and fall time. By using time-of-flight measurements, we propose a charge transport model in the H-Si NC film. For the proof-of-concept of this study, a flexible photodetector on a polyethylene terephthalate (PET) substrate is demonstrated by spin-coating colloidal H-Si NC solution in air. The photodetector can be bent in 5.9 mm bending radius at smallest and the device properly works after being bent in 2500 cycles.

Keywords: solution processing, silicon nanocrystal, photodetector, flexible electronics, time-of-flight, ligand-free

INTRODUCTION

Colloidal nanocrystals (NCs) are attractive in solution-processed electronic devices because a NC thin film can be formed on a flexible polymer film.[1–4] Traditional colloidal NCs are surface-passivated by organic ligands with long hydrocarbon chains. Organic ligands make NCs disperse in solution with steric hindrance and thus ligands are indispensable for colloidal NCs. However, long-chain organic ligands interrupt the charge carrier transport in a film produced from the solution.[2,5,6] Therefore, for the semiconductor device applications, further treatments to remove organic ligands are usually required.[7–9] Ideal surface ligands for high conductivity are inorganic ligands such as ionic complex. Kovalenko *et al.* demonstrated that the conductivity of a solution-processed gold (Au) NC film increased by 11 orders of magnitude by exchanging dodecanethiol organic ligands with $Sn_2S_6^{4-}$ inorganic ions.[7] The conductivity reached to 200 S/cm, which was much higher than that of a Au NC film with short-chain organic ligands. Similar strong improvement of the conductivity by controlling surface ligands has been reported for colloidal semiconductor NC films.[10–12]

Among many kinds of colloidal semiconductor NCs, colloidal silicon (Si) NCs have several advantages such as the high environmental-friendliness and the high compatibility with the current semiconductor technology.[13–15] A variety of electronic devices has been developed by using Si NC films: thin-film transistor (TFT)[16–18], light-emitting diode[19–25], solar cell[26–28], and photodetector[29,30]. A simple method to improve the conductivity of a Si NC film is sintering.[16,31] For example, Niesar et al. annealed a solution-processed Si NC film at 200 °C.[31] Although annealing improves the conductivity, it cannot be applied to non-thermal resistant polymer substrate such as polyethylene terephthalate (PET). Another approach to achieve a high conductivity in a solution-processed Si NC film is to use short inorganic ligands to reduce the

tunneling barriers between NCs.[17,29,32] Wheeler *et al*. synthesized chlorine (Cl)-terminated colloidal Si NCs in a glovebox and achieved high conductivity of the solution-processed Si NC film (2.5×10^{-5} S/cm) without annealing.[33] Erogbogbo *et al.* previously obtained dispersed ligand-free Si and Ge nanoparticle solution simply by using sonication and filteration.[34] Wheeler *et al.* have recently proposed that surface interaction between solvent molecules and boronated Si NC surface is responsible for the solubility of boron (B)-doped Si NCs in solvent.[35]

The shortest inorganic ligand in Si NCs is hydrogen (H). We can expect an efficient electronic coupling between H-terminated Si NCs (H-Si NCs) due to the short Si-H distance (≈ 0.15 nm[36]). However, H-Si NCs are strongly hydrophobic and the van der Waals interaction agglomerates them in polar liquids (water and alcohol).[37–39] Furthermore, solution dispersion by steric hindrance is not expected due to the small atomic radius. Therefore, in order to obtain a film of a H-Si NC, post-deposition treatments have been indispensable. Pereira *et al*. produced a H-Si NC film by immersing a film of natively oxidized Si NC in a dilute hydrofluoric acid (HF) solution to etch out the surface oxide.[32] The film conductivity was 3×10^{-7} S/cm and 5×10^{-9} S/cm in air and vacuum, respectively. Gresback *et al*. produced a TFT of H-Si NCs by exposing a film of Cl-terminated Si NCs to HF vapor. The TFT showed ≈ 10^{-6} S/cm in nitrogen ambient.[17] Although strong enhancement of the conductivity by HF solution or vapor has been demonstrated, it is desirable to avoid the harsh process for the development of practical electronic devices.

The purpose of this work is to produce a highly conductive film of H-Si NCs by a solution-based process without any post treatments in ambient air and study the electronic properties. We use a boron (B) and phosphorus (P) codoped Si NC solution developed in our group.[15,39,40] The Si NC is composed of a crystalline Si core and a highly B and P-concentrated Si shell.[39,41,42] The shell induces negative potential on the surface, which makes the Si NC dispersible in methanol

without organic ligands.[39] The dispersed NC solution is important for depositing an optically flat, crack-free, and flexible Si NC film.[43–45] Therefore, the Si NC is a unique material, which realizes solution dispersibility and H-termination simultaneously. First, we characterize basic current transport properties of a solution-processed H-Si NC film. The conductivity is evaluated as a function of time after film preparation. Variation of conductivity over a film is discussed. Then, we measure photocurrent of a H-Si NC thin film. By using time-of-flight (TOF) measurements, a charge transport model in a solution-processed H-Si NC film is discussed. Finally, we show the proof-of-concept to produce flexible electronic devices by using colloidal H-Si NCs: an air-stable and flexible photodetector on a PET film is demonstrated.

EXPERIMENTAL PROCEDURE

Preparation of colloidal H-Si NCs. Colloidal Si NCs were prepared by using a co-sputtering method described in our previous papers.[39–41,46] Si-rich borophosphosilicate films were deposited on a stainless steel plate by co-sputtering Si, SiO_2, B_2O_3 and P_2O_5. After removal from the steel plate, the films were annealed in a N_2 atmosphere to grow Si NCs. The annealing temperatures were 1100 and 1200 ^oC. The average diameter of Si NCs were 3.9 ± 1.2 and 6.9 ± 2.0 nm for 1100 and 1200 ^oC, respectively, which was previously evaluated by using transmission electron microscope (TEM) and dynamic light scattering measurements.[46] Then, the films were mixed with HF (46 wt %) to etch SiO_2 matrices and extract the Si NCs. After this process, Si NCs were H-terminated. The H-Si NCs were centrifuged and transferred into methanol under ambient air. The pH of the finished colloidal solution was 3. Immediately after the preparation of the solution, the NCs were deposited on substrates as explained later. The B and P concentration in Si NCs were estimated to be ~10 at.% and ~3 at. % by using inductively-coupled plasma atomic emission spectrometry (ICP-AES).[39] Note that most of B and P atoms are inactive and accumulated on the surface of NCs to form an inorganic shell.[42]

Absorption spectroscopy of H-Si NC thin film. Infrared (IR) and ultraviolet (UV)-Vis-near IR (NIR) absorption spectra of thin films were measured in air (Spectrum GX, PerkinElmer and UV-3101PC, Shimadzu). Si NC thin films were prepared on a gold-coated substrate and a silica substrate for IR and UV-vis-NIR absorption spectra, respectively.

Solution processing of H-Si NC thin film. A colloidal H-Si NC solution (~1 mg/mL) just after the HF etching (within 1 hour) was spin-coated on substrates. Note that all the processes were performed in an ambient air and a glove-box was not used during the whole process. Substrates

were cleaned up by ultrasonication with alcohol and UV/O_3 treatments. Top electrodes were fabricated by using thermal evaporation (aluminum: Al) or rf-sputtering (indium-tin-oxide: ITO) with a metal mask after spin-coating. The diameter of the top electrodes was approximately 1 mm.

Electrical characterization. A layer structure of the Al/Si NC thin film (*D*=3.9 nm)/ITO coated glass (GEOMATECH, surface resistivity: <10 Ω/sq) was used for basic electrical characterization of Si NC thin films. Thickness of the film was 65 nm, which was evaluated by using a stylus profiler. Current-voltage characteristics were taken by a source measure unit (236, Keithley). Impedance spectroscopy was taken by using an LCR meter (ZM2376, NF Corporation). Static photocurrent measurements were carried out with a 405 nm semiconductor laser module (CUBE, Coherent Inc.) with TTL modulation and an oscilloscope (DS-5634-A, Iwatsu).

TOF measurement. A layer structure of the ITO/Si NC film (*D*=6.9 nm)/Au coated glass was used for TOF measurements. Thickness of the Si NC film estimated using a stylus profiler was in the range from 900 nm to 1.2 μm (Figure S1). A 355 nm third harmonic wave of a Nd:YAG laser (Quanta-Ray INDI, Spectra-Physics: pulse duration 10 ns, repetition frequency 20 Hz) was used for transient photocurrent measurements. The measurements were carried out with the oscilloscope and a source measure unit (2400 and 236, Keithley) in a cryostat. A load resistor 100 kΩ was used to convert a transient photocurrent to a voltage which was measured in the oscilloscope.

Flexible Si NC photodetector on PET film. A layer structure of the Al/Si NC thin film (*D*=3.9 nm)/ITO coated PET film (Aldrich, surface resistivity: 60 Ω/sq, 127 μm in thickness) was fabricated. Mechanical stability was evaluated by folding the photodetector on glass vials with various bending radii. EQE of the photodetector was evaluated by using the source measure unit and a monochromatized light from a spectrophotometer (Fluorolog-3, Horiba Jovin Yvon).

RESULTS AND DISCUSSION

Figure 1(a) shows a photo of colloidal Si NC solution in this study. Colloidal Si NCs are clearly dispersed in methanol. Figure 1(b) shows TEM (JEM-2100F, JEOL) images of Si NCs (anneal temperature: 1100 ^{o}C). The high-resolution TEM image in the inset gives a lattice fringe of Si, which guarantees a high crystallinity of NCs. Figure 1(c) shows IR absorption spectra of Si NC films as a function of age of colloidal H-Si NC solution in methanol. The storage and deposition of Si NC solution were in air without any special treatments. In this study, the age means the time after the end of preparation of the Si NC solution (See Experimental procedure). The films are prepared by drop-casting NC solution in air. In the spectrum of 6-hours age, absorption of Si-H stretching mode (v(Si-H)) is stronger than that of Si-O-Si asymmetric stretching mode (v(Si-O-Si)), which indicates that H-termination on colloidal NC surface is mostly kept within 6 hours in ambient air. Absorption of v(Si-O-Si) increases as colloidal solution is aged due to native surface oxidation in methanol. All of the Si NC films for electrical measurements are prepared by using Si NCs within the age of 1 hour.

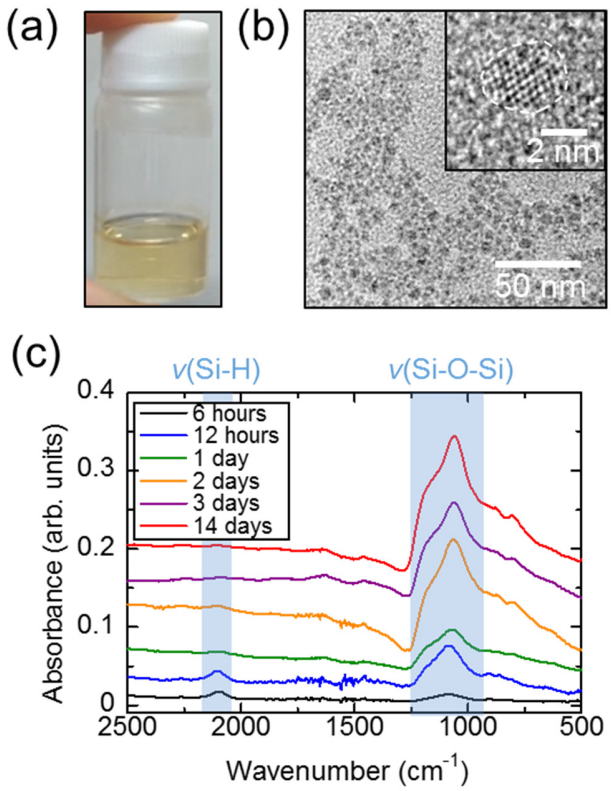

Figure 1. (a) Photo of colloidal silicon nanocrystals in methanol. (b) TEM image of silicon nanocrystals. Inset: high-resolution TEM image. (c) IR spectra of Si NC films as a function of age of colloidal H-Si NC solution. The spectra are offset for clarity.

Figure 2(a) is a schematic illustration of a layer structure for electrical characterization of a H-Si NC film. A spin-coated Si NC thin film is sandwiched by ITO and Al electrodes. The diameter of Al electrodes is ≈ 1 mm. Figure 2(b) shows conductivity on a H-Si NC thin film after film preparation. The conductivity is measured in vacuum but exposed to ambient air between the measurements. The conductivity of an as-deposited H-Si NC thin film (0 day) is 2×10^{-5} S/cm, which is comparable to the reported high conductivity of a Cl-terminated Si NC film in vacuum and inert gas condition (red triangle).[17,33] Even after 277 days (≈ 9 months), the conductivity of a H-Si NC thin film is at 10^{-7} S/cm. This value is close to previous reported conductivity of a fresh H-Si NC film in air (blue square).[32] It is noted that the conductance of a H-Si NC film is six orders of magnitude larger than that of a film made from natively oxidized Si NCs in methanol. This result suggests that current transport pathways are maintained when a freshly prepared NC film is oxidized. Native oxidation of NCs does not largely degrade the pathways between NCs in an array. In order to evaluate the variation of conductivity over a H-Si NC film, we measure 28 points on a same as-deposited H-Si NC film. The area of the film is 100 mm^2. Figure 2(c) shows the distribution of conductivity at 1 V. Average conductivity is ≈ 10^{-5} S/cm. This figure indicates that a uniform H-Si NC film of 100 mm^2 can be prepared by spin-coating the colloidal solution in air.

Figure 2(d) shows the result of impedance (Z) spectroscopy in a H-Si NC film. According to the Cole-Cole plot, the resistance and capacitance of a H-Si NC film are R=894 Ω and C=1.76 nF, respectively. The time constant of the thin film is $\tau = RC$=1.57 μs. In the same structure using an natively oxidized Si NC thin film, the time constant was 3 s.[44] Therefore, the time constant is improved by six orders of magnitude using a H-Si NC thin film. Frequency dependence of Z in Figure 2(e) indicates that the film can follow more than 10 kHz modulation.

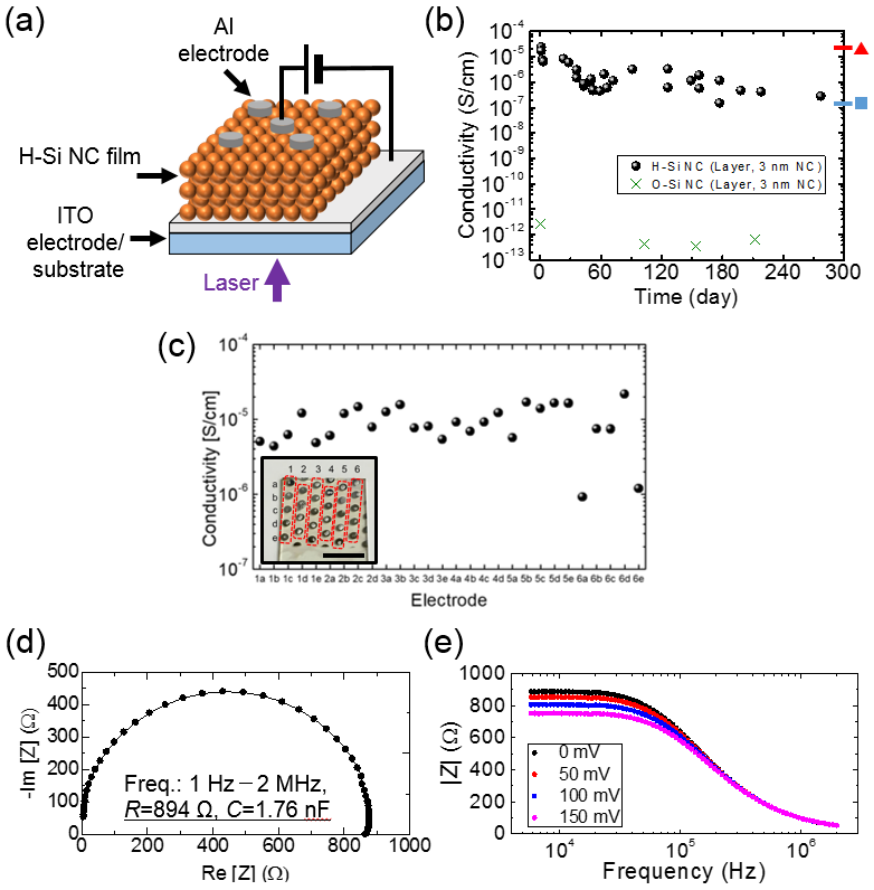

Figure 2. (a) Schematic of a layer structure for electrical characterization of H-Si NC film. (b) Conductivity of H-Si NC films as a function of time after film preparation. Values of reported Si NC film conductivity in vacuum[33] and air[32] are also shown as red triangle and blue square in the right axis, respectively. (c) Variation of conductivity on a H-Si NC film. Inset photo shows measurement points on a film. We measured 28 points on a film as noted dashed rectangles. Scale bar is 5 mm. (d) Impedance plot of a H-Si NC film. (e) Frequency dependence of impedance.

Current under 405 nm laser irradiation (24 mW) is shown in Figure 3(a). Conductance of the H-Si NC thin film increases under the laser irradiation. Figure 3(b) shows a log-log plot of H-Si NC current under dark. The slope of the log-log curve is 1.0 at voltages smaller than 0.1 V, which indicates Ohmic transport. At this region, conductivity is 8.2×10^{-8} S/cm. On the contrary, current at voltages larger than 0.3 V is non-linear and the slope is 3.8. This tendency is consistent with the high conductive Si NC films in the previous reports.[32,33]

Figure 3(c) shows a power dependence on 405 nm laser of short-circuit current (i.e., current under zero voltage). In general, a photocurrent I_{ph} increases with light power intensity P following a power law $I_{ph} \propto P^{\gamma}$. The values of γ are 0.95 and 0.87 in vacuum and air, respectively. Pereira et al. reported the values of γ in a H-Si NC film using planar electrodes changed from 0.97 (vacuum) to 0.57 (air). [32] In our H-Si NC film, current-transport is not largely affected by air because the top Al electrode works as a passivation layer. Figure 3(d) shows response of short-circuit current to 4 kHz-modulated laser irradiation (405 nm, 4.6 mW). Rise and fall time are 6.8 and 24.1 μs by fitting an exponential curve to the response (Figure 3(e)). These values are longer than the time constant obtained from the impedance spectroscopy (1.57 μs) in Figure 2(d). A photo-excitation process in the Si NC film possibly limits the photocurrent response, although we do not have experimental data to prove it. Fast response time of ≈ 10 μs has been reported on a graphene/sputtered Si quantum dot heterojunction diode.[47] A H-Si NC film has a potential to fabricate a similar fast-response flexible photodetector.

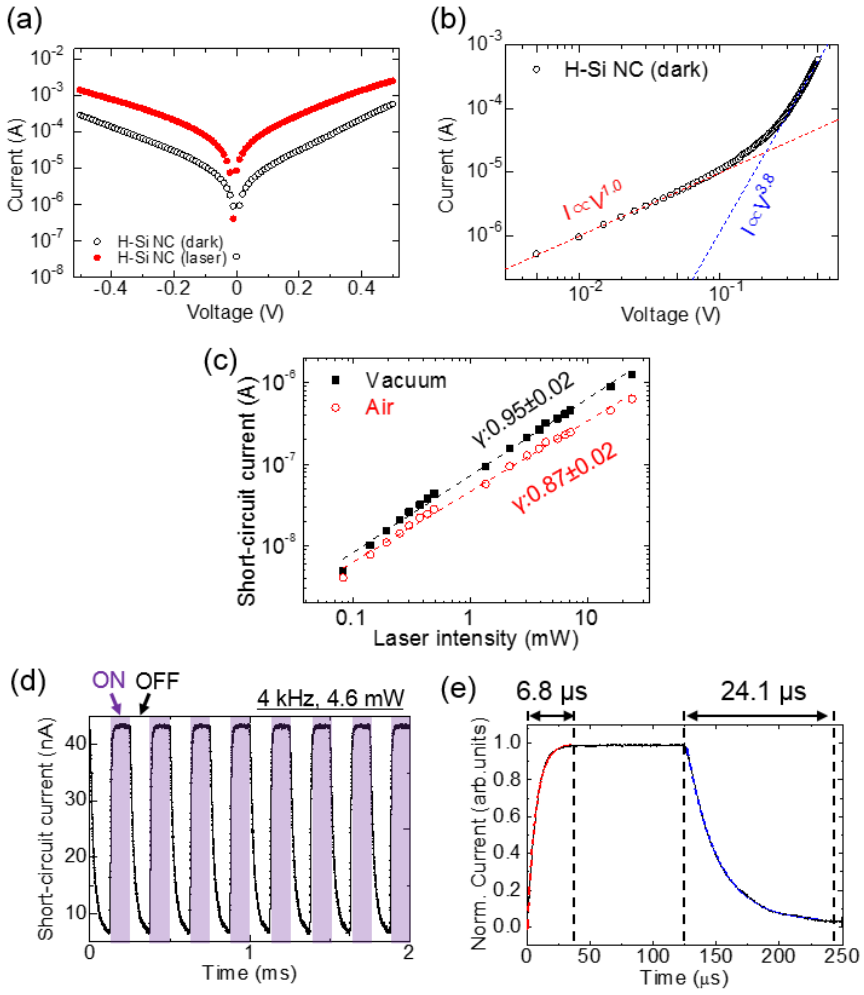

Figure 3. (a) Current-voltage characteristics of H-Si NC current under dark and 405 nm irradiation (24 mW). (b) A log-log plot of H-Si NC current under dark. (c) Short-circuit current as a function of 405 nm laser intensity in vacuum and air. (d) Short-circuit current in 4 kHz modulated laser irradiation (4.6 mW) and (e) Rise and fall time of short-circuit current. Response and recovery time are evaluated by exponential fitting.

In order to elucidate carrier transport mechanism on a solution-processed H-Si NC film, a TOF measurement is carried out. Figure 4(a) shows an UV-vis-NIR absorption spectrum of a Si NC film on a silica substrate. Thickness of the film is 300 nm. Light in shorter wavelength is much absorbed, which corresponds to direct transition of electrons in Si. For generating a charge sheet in a NC thin film, we choose a 355-nm pulse laser and a 900-nm thick Si NC film. In TOF measurement, an ITO/Si NC film/Au layer structure is used. The voltage is applied to an ITO electrode and the pulse laser is irradiated through the ITO electrode. This configuration can measure a hole mobility because photo-generated holes near the ITO electrode are moved to the opposite Au electrode (see the inset illustration in Figure 4(b)).

Figure 4(b) shows transient photocurrent spectra as a function of applied voltages. The inflected spectra are explained by using a dispersive charge transport mechanism: multiple traps disperse a photo-excited carrier packet during transport[48]. This mechanism has been discussed in amorphous semiconductor[49], organic semiconductor[50], and nanoparticle films[51–53]. Our Si-NC thin film also has a dispersive charge transport because energy levels of NCs have a distribution due to size dispersion as discussed later[54,55].

We determine the transit time τ_{tr} by using Figure 4(b). The value of τ_{tr} is extracted from the inflection point of a photocurrent decay curve.[53,56] The values of τ_{tr} are 40—100 μs under 97.1—118.9 V. Inverse of τ_{tr} in each voltage is shown in Figure 4(c). According to a basic theory of the TOF measurement, τ_{tr} is related to the applied voltage V as $1/\tau_{tr} = (\mu/t^2)V$ where μ is the carrier mobility and t is the thickness of the film.[57] Although the thickness of the film is fluctuated in the range from 900 nm to 1.2 μm, we employ t = 900 nm for the analysis because the electrical transport is dominated by the thinnest area of the film. Therefore, we can estimate the carrier mobility from the slope of voltage dependence of $1/\tau_{tr}$. When the voltage is higher

(lower) than 100 V (electric field: 1.1 MV/cm), μ is 4.9×10^{-6} (5.4×10^{-7}) cm^2/Vs. The dependence of μ indicates that the carrier transport mechanism changes at the electric field, although details are not clarified. Temperature dependence of a hole mobility is shown in Figure 4(d). The mobility is calculated by using a temperature dependence of $1/\tau_{tr}$ versus voltage in Figure S2. The hole transport through a H-Si NC film requires an activation energy E_A = 45 meV, which is evaluated by using the Arrhenius plot.

In order to find a field-effect mobility in a TFT, we have also fabricated a solution-processed TFT using a 6.9 nm-diameter Si NC film. As shown in the inset in Figure 4(e), a bottom-contact and bottom-gate TFT is fabricated by using gold interdigitated electrodes (separation: 20 μm) on a thermally oxidized silicon substrate (SiO_2 thickness: 90 nm). The TFT shows p-type behaviors in vacuum at room temperature. Hole is thus the majority carrier in this Si NC film. This result is consistent with the energy level diagrams of B and P codoped Si NC films obtained by photoelectron yield spectroscopy and X-ray photoelectron spectroscopy: the Fermi level is close to the highest occupied molecular orbital (HOMO) level.[54] The hole field-effect mobility μ is calculated to be 2.2×10^{-7} cm^2/Vs by using TFT operation in a linear region. This mobility is consistent with the value of μ in Figure 4(c). The mobility is much smaller than those of bulk Si crystal and high-mobility compound semiconductor NC films (> 10 cm^2/Vs).[2,3]

We discuss a charge transport model in a H-Si NC thin film as follows. Figure 4(f) shows schematic illustration of charge transport in a H-Si NC film. In two adjacent NCs, carrier transport from i^{th} NC to i+1^{th} NC through the highest occupied molecular orbital (HOMO) and the lowest unoccupied molecular orbital (LUMO) is dominated by a tunneling rate $\Gamma_{i,i+1}$ described as:

$$\Gamma_{i,i+1} \propto \exp(-\beta\Delta x)\exp\left(-\frac{E_k^{i+1}-E_k^{i}}{k_B T}\right) \qquad (E_{LUMO}^{i} < E_{LUMO}^{i+1}, E_{HOMO}^{i} > E_{HOMO}^{i+1}),$$

$$\Gamma_{i,i+1} \propto \exp(-\beta\Delta x) \qquad (E^{i}_{\mathrm{LUMO}} \geq E^{i+1}_{\mathrm{LUMO}}, E^{i}_{\mathrm{HOMO}} \leq E^{i+1}_{\mathrm{HOMO}}),$$

where β is the tunneling decay constant, Δx is the shortest edge-to-edge distance between the NCs, E^{i}_{k} is the energy level of i^{th} NCs versus vacuum level (k=HOMO or LUMO: see the definition in Figure 4(f)), k_{B} is the Boltzmann constant, and T is the temparature.[9,58] This equation theoretically suggests that we can expect larger $\Gamma_{i,i+1}$ in a solution-processed H-Si NC film due to reducing Δx. A H-Si NC thin film has energy level distribution due to size dispersion. In our previous study, the HOMO and LUMO levels of a Si NC film have a distribution with approximately 100 meV.[54] Thus, energy level difference between adjacent NCs $E^{i+1}_{\mathrm{k}} - E^{i}_{\mathrm{k}}$ is expected to be 100 meV at maximum. This energy level difference possibly results in E_{A}=45 meV in Figure 4(d).

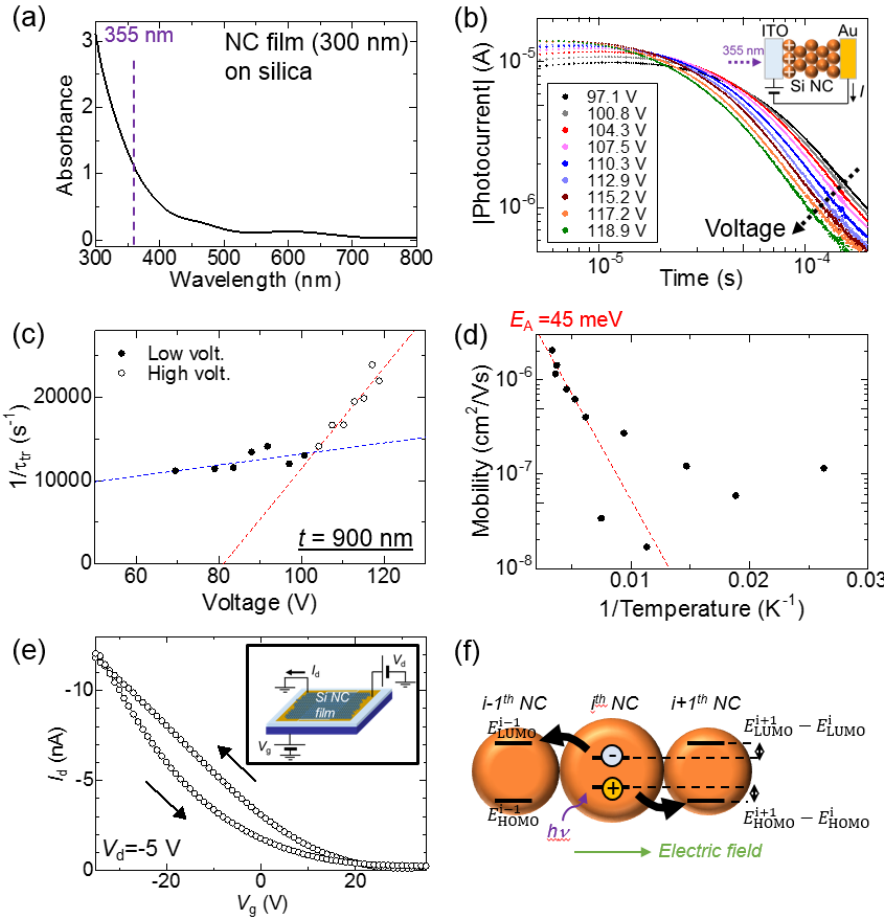

Figure 4. (a) Absorption spectrum of a hydrogen terminated Si-NC thin film (D=6.9 nm) on silica glass. (b) Transient photocurrent under various bias voltages (97.1 – 118.9 V). Inset shows a circuit diagram of a TOF measurement. (c) Inverse of transient time as a function of bias voltages. The red (blue) dashed line is a linear fitting for mobility calculation in a higher (lower) voltage region. (d) Hole mobility as a function of temperatures. (e) Drain current (I_d) versus gate voltage (V_g) characteristic of a solution-processed Si NC TFT is shown. Inset: schematic of Si NC TFT. (f) Schematic illustration of charge transport in a H-Si NC thin film.

Finally, we prove our concept in this study: producing flexible electronic devices by using colloidal H-Si NCs. Here, we demonstrate an air-stable flexible photodetector. The Si NC film is also spin-coated on a PET substrate in ambient air. The photodetector is bendable as shown in Figure 5(a). A current-voltage curve of a H-Si NC thin film on a PET substrate is similar to that on a glass substrate (Figure S3). Furthermore, we observed slow degradation of the conductivity on a PET substrate, which is also similar to that on a glass substrate (Figure S4). An external quantum efficiency (EQE) of a H-Si NC thin film as a function of irradiated photon wavelength is shown in Figure 5(b). The value of EQE is larger at shorter wavelength, and therefore, this device works as a UV photodetector. Responsivity of the flexible photodetector R = EQE × (λ[nm]/1240) is calculated to be 2.3×10^{-2} A/W at λ=360 nm under 5 mV application (Figure S5), which is comparable to previous colloidal Si NC photodetectors on a solid glass and a silicon substrate.[29,47] Figure 5(c) shows photocurrent and dark current as a function of bending radius. The photodetector clearly operates in 5.9－17.5 mm bending radius. A ratio of photocurrent and dark current is 100 in both flat and bent condition. Figure 5(d) shows photocurrent stability after bending cycles. We have confirmed that the photodetector shows a stable current after a 2500-cycles bending trial. It should be noted that the measurements are carried out in air, and therefore the flexible photodetector is air-stable.

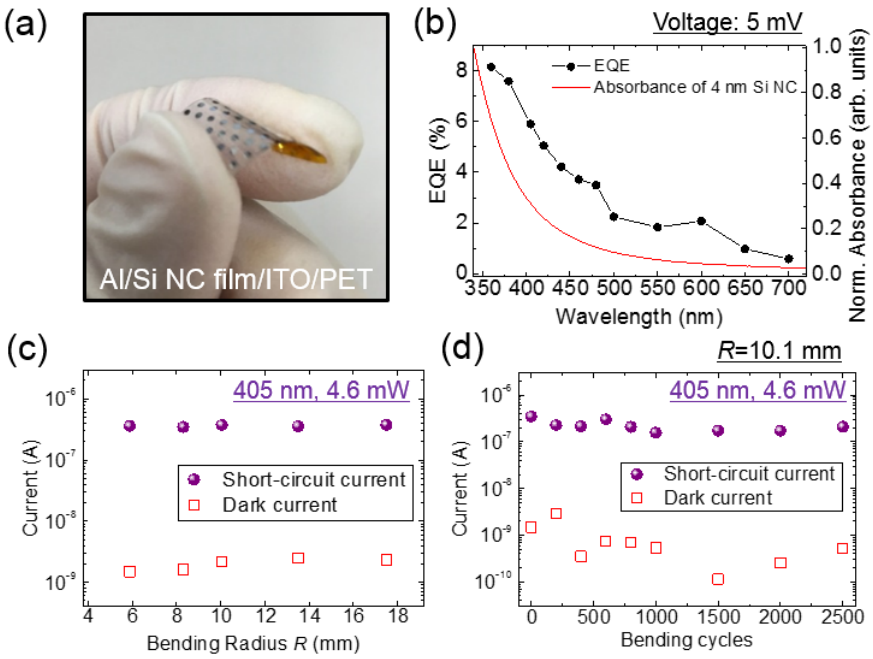

Figure 5. (a) Picture of a bent Al/H-Si NC film/ITO/PET film. (b) EQE as a function of irradiated photon wavelength. Absorption spectrum of H-Si NCs (D=3.9 nm) is also shown. (c) Photocurrent intensity as a function of bending radius. (d) Photocurrent intensity as a function of bending cycles.

CONCLUSIONS

For flexible electronic devices, we have demonstrated the concept to produce a conductive solution-processed Si NC film by using colloidal H-Si NCs. We used colloidal H-Si NCs which have solution dispersibility and H-termination simultaneously. The solution-processed H-Si NC film in air showed conductivity 2×10^{-5} S/cm, which was comparable to reported conductivity of Si NC films prepared in inert atmosphere. The conductivity was maintained at $\approx 10^{-7}$ S/cm in 9 months after fabrication and was uniform over the spin-coated Si NC (100 mm^2). The film showed 6.8 and 24.1 μs of rise and fall time to laser irradiation. By using TOF measurements, we discussed a charge transport model in the H-Si NC film. The photodetector on a PET substrate was demonstrated by spin-coating colloidal H-Si NC solution in air. The photodetector was able to be bent in 5.9 mm bending radius at smallest and properly worked after being bent in 2500 cycles. Solution processing of colloidal H-Si NC solution can be a promising method for flexible electronic devices.

ASSOCIATED CONTENT

Supporting Information.

This material is available free of charge via the Internet at http://pubs.acs.org. Thickness evaluation of the Si NC film; temperature dependence of inverse of transit time; current-voltage characteristics of H-Si NC films on glass and PET substrates; current-voltage characteristics of a Si NC film on a PET substrate kept for 6 months; responsivity of a UV photodetector using H-Si NC.

Corresponding Author

*to whom correspondence should be addressed. Email: kano@eedept.kobe-u.ac.jp.

ACKNOWLEDGMENT

The authors acknowledge Dr H. Sugimoto for observation of TEM images. This work was partly supported by JSPS KAKENHI Grant Number 16H03828, JST Visegrad Group (V4)-Japan Joint Research Program (Advanced Materials), and Kawanishi Memorial ShinMaywa Education Foundation. The authors acknowledge Hyogo Prefectural Institute of Technology to use a stylus profiler.

REFERENCES

(1) Talapin, D. V.; Lee, J.-S.; Kovalenko, M. V.; Shevchenko, E. V. Prospects of Colloidal Nanocrystals for Electronic and Optoelectronic Applications. *Chem. Rev.* **2010**, *110*, 389–458.

(2) Kovalenko, M. V; Manna, L.; Cabot, A.; Hens, Z.; Talapin, D. V; Kagan, C. R.; Klimov, X. V. I.; Rogach, A. L.; Reiss, P.; Milliron, D. J.; Guyot-sionnnest, P.; Konstantatos, G.; Parak, W. J.; Hyeon, T.; Korgel, B. A.; Murray, C. B.; Heiss, W. Prospects of Nanoscience with Nanocrystals. *ACS Nano* **2015**, *9* (2), 1012–1057.

(3) Kagan, C. R.; Lifshitz, E.; Sargent, E. H.; Talapin, D. V. Building Devices from Colloidal Quantum Dots. *Science (80-.).* **2016**, *353* (6302), aac5523-aac5523.

(4) Choi, J.-H.; Wang, H.; Oh, S. J.; Paik, T.; Jo, P. S.; Sung, J.; Ye, X.; Zhao, T.; Diroll, B. T.; Murray, C. B.; Kagan, C. R. Exploiting the Colloidal Nanocrystal Library to Construct Electronic Devices. *Science (80-.).* **2016**, *352* (6282), 205–208.

(5) Klinke, C. Electrical Transport through Self-Assembled Colloidal Nanomaterials and Their Perspectives. *Epl* **2017**, *119* (3), 0–6.

(6) Boles, M. A.; Ling, D.; Hyeon, T.; Talapin, D. V. The Surface Science of Nanocrystals. *Nat. Mater.* **2016**, *15* (2), 141–153.

(7) Kovalenko, M. V; Scheele, M.; Talapin, D. V. Colloidal Nanocrystals with Molecular Metal Chalcogenide Surface Ligands. *Science (80-.).* **2009**, *324* (5933), 1417–1420.

(8) Kagan, C. R.; Murray, C. B. Charge Transport in Strongly Coupled Quantum Dot Solids. *Nat. Nanotechnol.* **2015**, *10*, 1013–1026.

(9) Guyot-Sionnest, P. Electrical Transport in Colloidal Quantum Dot Films. *J. Phys. Chem. Lett.* **2012**, *3* (9), 1169–1175.

(10) Nag, A.; Chung, D. S.; Dolzhnikov, D. S.; Nada, M.; Chattopadhyay, S.; Shibata, T.; Talapin, D. V. The Effect of Metal Ions on Photoluminescence , Charge Transport , Magnetic and Catalytic Properties of All- Inorganic Colloidal Nanocrystals and Nanocrystal Solids The Effect of Metal Ions on Photoluminescence , Charge Transport , Magnetic and Catalytic. *J. Am. Chem. Soc.* **2012**, *134*, 13604–13615.

(11) Dolzhnikov, D. S.; Zhang, H.; Jang, J.; Son, J. S.; Panthani, M. G.; Shibata, T.; Chattopadhyay, S.; Talapin, D. V. Composition-Matched Molecular “solders” for Semiconductors. *Science (80-.).* **2015**, *347* (6220), 425–428.

(12) Wheeler, L. M.; Nichols, A. W.; Chernomordik, B. D.; Anderson, N. C.; Beard, M. C.; Neale, N. R. All-Inorganic Germanium Nanocrystal Films by Cationic Ligand Exchange. *Nano Lett.* **2016**, *16* (3), 1949–1954.

(13) McVey, B. F. P.; Tilley, R. D. Solution Synthesis, Optical Properties, and Bioimaging Applications of Silicon Nanocrystals. *Acc. Chem. Res.* **2014**, *47* (10), 3045–3051.

(14) Reiss, P.; Carriere, M.; Lincheneau, C.; Vaure, L.; Tamang, S. Synthesis of Semiconductor Nanocrystals, Focusing on Nontoxic and Earth-Abundant Materials. *Chem. Rev.* **2016**, *116* (18), 10731–10819.

(15) Fujii, M.; Sugimoto, H.; Imakita, K. All-Inorganic Colloidal Silicon Nanocrystals—surface Modification by Boron and Phosphorus Co-Doping. *Nanotechnology* **2016**, *27* (26), 262001.

(16) Holman, Z. C.; Liu, C.-Y.; Kortshagen, U. R. Germanium and Silicon Nanocrystal Thin-Film Field-Effect Transistors from Solution. *Nano Lett.* **2010**, *10* (7), 2661–2666.

(17) Gresback, R.; Kramer, N. J.; Ding, Y.; Chen, T.; Kortshagen, U. R.; Nozaki, T. Controlled Doping of Silicon Nanocrystals Investigated by Solution-Processed Field Effect Transistors. *ACS Nano* **2014**, *8* (6), 5650–5656.

(18) Pereira, R. N.; Coutinho, J.; Niesar, S.; Oliveira, T. A.; Aigner, W.; Wiggers, H.; Rayson, M. J.; Briddon, P. R.; Brandt, M. S.; Stutzmann, M. Resonant Electronic Coupling Enabled by Small Molecules in Nanocrystal Solids. *Nano Lett.* **2014**, *14* (7), 3817–3826.

(19) Maier-Flaig, F.; Rinck, J.; Stephan, M.; Bocksrocker, T.; Bruns, M.; Kübel, C.; Powell, A. K.; Ozin, G. A.; Lemmer, U. Multicolor Silicon Light-Emitting Diodes (SiLEDs). *Nano Lett.* **2013**, *13*, 475–480.

(20) Ghosh, B.; Masuda, Y.; Wakayama, Y.; Imanaka, Y.; Inoue, J. I.; Hashi, K.; Deguchi, K.; Yamada, H.; Sakka, Y.; Ohki, S.; Shimizu, T.; Shirahata, N. Hybrid White Light Emitting Diode Based on Silicon Nanocrystals. *Adv. Funct. Mater.* **2014**, *24* (45), 7151–7160.

(21) Cheng, K. Y.; Anthony, R.; Kortshagen, U. R.; Holmes, R. J. Hybrid Silicon Nanocrystal-Organic Light-Emitting Devices for Infrared Electroluminescence. *Nano Lett.* **2010**, *10* (4), 1154–1157.

(22) Liu, X.; Zhao, S.; Gu, W.; Zhang, Y.; Qiao, X.; Ni, Z.; Pi, X.; Yang, D. Light-Emitting Diodes Based on Colloidal Silicon Quantum Dots with Octyl and Phenylpropyl Ligands. *ACS Appl. Mater. Interfaces* **2018**, *10* (6), 5959–5966.

(23) Cheng, K. Y.; Anthony, R.; Kortshagen, U. R.; Holmes, R. J. High-Efficiency Silicon Nanocrystal Light-Emitting Devices. *Nano Lett.* **2011**, *11* (5), 1952–1956.

(24) Puzzo, D. P.; Henderson, E. J.; Helander, M. G.; Wang, Z.; Ozin, G. a.; Lu, Z. Visible Colloidal Nanocrystal Silicon Light-Emitting Diode. *Nano Lett.* **2011**, *11*, 1585–1590.

(25) Mastronardi, M. L.; Henderson, E. J.; Puzzo, D. P.; Chang, Y.; Wang, Z. Bin; Helander, M. G.; Jeong, J.; Kherani, N. P.; Lu, Z.; Ozin, G. a. Silicon Nanocrystal OLEDs: Effect of Organic Capping Group on Performance. *Small* **2012**, *8* (23), 3647–3654.

(26) Liu, C. Y.; Kortshagen, U. R. A Silicon Nanocrystal Schottky Junction Solar Cell Produced from Colloidal Silicon Nanocrystals. *Nanoscale Res. Lett.* **2010**, *5* (8), 1253–1256.

(27) Liu, C.-Y.; Holman, Z.; Kortshagen, U. Hybrid Solar Cells from P3HT and Silicon Nanocrystals. *Nano Lett.* **2009**, *9* (1), 449–452.

(28) Ding, Y.; Sugaya, M.; Liu, Q.; Zhou, S.; Nozaki, T. Oxygen Passivation of Silicon Nanocrystals: Influences on Trap States, Electron Mobility, and Hybrid Solar Cell Performance. *Nano Energy* **2014**, *10*, 322–328.

(29) Lin, T.; Liu, X.; Zhou, B.; Zhan, Z.; Cartwright, A. N.; Swihart, M. T. A Solution-Processed UV-Sensitive Photodiode Produced Using a New Silicon Nanocrystal Ink. *Adv. Funct. Mater.* **2014**, *24* (38), 6016–6022.

(30) Ni, Z.; Ma, L.; Du, S.; Xu, Y.; Yuan, M.; Fang, H.; Wang, Z.; Xu, M.; Li, D.; Yang, J.; Hu, W.; Pi, X.; Yang, D. Plasmonic Silicon Quantum Dots Enabled High-Sensitivity Ultrabroadband Photodetection of Graphene-Based Hybrid Phototransistors. *ACS Nano* **2017**, *11* (10), 9854–9862.

(31) Niesar, S.; Pereira, R. N.; Stegner, A. R.; Erhard, N.; Hoeb, M.; Baumer, A.; Wiggers, H.; Brandt, M. S.; Stutzmann, M. Low-Cost Post-Growth Treatments of Crystalline Silicon Nanoparticles Improving Surface and Electronic Properties. *Adv. Funct. Mater.* **2012**, *22* (6), 1190–1198.

(32) Pereira, R. N.; Niesar, S.; You, W. B.; Da Cunha, a. F.; Erhard, N.; Stegner, a. R.; Wiggers, H.; Willinger, M. G.; Stutzmann, M.; Brandt, M. S. Solution-Processed Networks of Silicon Nanocrystals: The Role of Internanocrystal Medium on Semiconducting Behavior. *J. Phys. Chem. C* **2011**, *115*, 20120–20127.

(33) Wheeler, L. M.; Neale, N. R.; Chen, T.; Kortshagen, U. R. Hypervalent Surface Interactions for Colloidal Stability and Doping of Silicon Nanocrystals. *Nat. Commun.* **2013**, *4*, 2197.

(34) Erogbogbo, F.; Liu, T.; Ramadurai, N.; Tuccarione, P.; Lai, L.; Swihart, M. T.; Prasad, P. N. Creating Ligand-Free Silicon Germanium Alloy Nanocrystal Inks. *ACS Nano* **2011**, *5* (10), 7950–7959.

(35) Wheeler, L. M.; Kramer, N. J.; Kortshagen, U. R. Thermodynamic Driving Force in the Spontaneous Formation of Inorganic Nanoparticle Solutions. *Nano Lett.* **2018**, *18* (3), 1888–1895.

(36) Bacalis, N. C.; Zdetsis, A. D. Properties of Hydrogen Terminated Silicon Nanocrystals via a Transferable Tight-Binding Hamiltonian, Based on Ab-Initio Results. *J. Math. Chem.* **2009**, *46* (3), 962–970.

(37) Sato, S.; Swihart, M. T. Propionic-Acid-Terminated Silicon Nanoparticles: Synthesis and Optical Characterization. *Chem. Mater.* **2006**, *18* (17), 4083–4088.

(38) Gupta, A.; Swihart, M. T.; Wiggers, H. Luminescent Colloidal Dispersion of Silicon Quantum Dots from Microwave Plasma Synthesis: Exploring the Photoluminescence Behavior across the Visible Spectrum. *Adv. Funct. Mater.* **2009**, *19* (5), 696–703.

(39) Sugimoto, H.; Fujii, M.; Imakita, K.; Hayashi, S.; Akamatsu, K. All-Inorganic near-Infrared Luminescent Colloidal Silicon Nanocrystals: High Dispersibility in Polar Liquid by Phosphorus and Boron Codoping. *J. Phys. Chem. C* **2012**, *116*, 17969–17974.

(40) Fukuda, M.; Fujii, M.; Sugimoto, H.; Imakita, K.; Hayashi, S. Surfactant-Free Solution-Dispersible Si Nanocrystals Surface Modification by Impurity Control. *Opt. Lett.* **2011**, *36* (20), 4026–4028.

(41) Sugimoto, H.; Fujii, M.; Imakita, K.; Hayashi, S.; Akamatsu, K. Phosphorus and Boron Codoped Colloidal Silicon Nanocrystals with Inorganic Atomic Ligands. *J. Phys. Chem. C* **2013**, *117*, 6807–6813.

(42) Nomoto, K.; Sugimoto, H.; Breen, A.; Ceguerra, A. V; Kanno, T.; Ringer, S. P.; Wurfl, I. P.; Conibeer, G. J.; Fujii, M. Atom Probe Tomography Analysis of Boron And/or Phosphorus Distribution in Doped Silicon Nanocrystals. *J. Phys. Chem. C* **2016**, *120*, 17845–17852.

(43) Sasaki, M.; Kano, S.; Sugimoto, H.; Imakita, K.; Fujii, M. Surface Structure and Current Transport Property of Boron and Phosphorous Co-Doped Silicon Nanocrystals. *J. Phys. Chem. C* **2016**, *120* (1), 195–200.

(44) Kano, S.; Sasaki, M.; Fujii, M. Combined Analysis of Energy Band Diagram and Equivalent Circuit on Nanocrystal Solid. *J. Appl. Phys.* **2016**, *119* (21), 215304.

(45) Kano, S.; Kim, K.; Fujii, M. Fast-Response and Flexible Nanocrystal-Based Humidity Sensor for Monitoring Human Respiration and Water Evaporation on Skin. *ACS Sensors* **2017**, *2*, 828–833.

(46) Sugimoto, H.; Fujii, M.; Imakita, K.; Hayashi, S.; Akamatsu, K. Codoping N- and P-Type Impurities in Colloidal Silicon Nanocrystals: Controlling Luminescence Energy from below Bulk Band Gap to Visible Range. *J. Phys. Chem. C* **2013**, *117* (22), 11850–11857.

(47) Shin, D. H.; Kim, S.; Kim, J. M.; Jang, C. W.; Kim, J. H.; Lee, K. W.; Kim, J.; Oh, S. D.; Lee, D. H.; Kang, S. S.; Kim, C. O.; Choi, S. H.; Kim, K. J. Graphene/Si-Quantum-Dot Heterojunction Diodes Showing High Photosensitivity Compatible with Quantum Confinement Effect. *Adv. Mater.* **2015**, *27* (16), 2614–2620.

(48) Scher, H.; Montroll, E. N. Anomalous Transit-Time Dispersion in Amorphous Solids. *Phys. Rev. B* **1975**, *12*, 2455.

(49) Spear, W. E. The Study of Transport and Related Properties of Amorphous Silicon by Transient Experiments. *J. Non. Cryst. Solids* **1983**, *59–60*, 1–13.

(50) O'Neill, M.; Kelly, S. M. Ordered Materials for Organic Electronics and Photonics. *Adv. Mater.* **2011**, *23* (5), 566–584.

(51) Johnston, K. W.; Pattantyus-Abraham, A. G.; Clifford, J. P.; Myrskog, S. H.; Hoogland, S.; Shukla, H.; Klem, E. J. D.; Levina, L.; Sargent, E. H. Efficient Schottky-Quantum-Dot Photovoltaics: The Roles of Depletion, Drift, and Diffusion. *Appl. Phys. Lett.* **2008**, *92* (12), 1–3.

(52) Ip, A. H.; Thon, S. M.; Hoogland, S.; Voznyy, O.; Zhitomirsky, D.; Debnath, R.; Levina, L.; Rollny, L. R.; Carey, G. H.; Fischer, A.; Kemp, K. W.; Kramer, I. J.; Ning, Z.; Labelle, A. J.; Chou, K. W.; Amassian, A.; Sargent, E. H. Hybrid Passivated Colloidal Quantum Dot Solids. *Nat. Nanotechnol.* **2012**, *7* (9), 577–582.

(53) Yazdani, N.; Bozyigit, D.; Yarema, O.; Yarema, M.; Wood, V. Hole Mobility in Nanocrystal Solids as a Function of Constituent Nanocrystal Size. *J. Phys. Chem. Lett.* **2014**, *5* (20), 3522–3527.

(54) Hori, Y.; Kano, S.; Sugimoto, H.; Imakita, K.; Fujii, M. Size-Dependence of Acceptor and Donor Levels of Boron and Phosphorus Codoped Colloidal Silicon Nanocrystals. *Nano Lett.* **2016**, *16* (4), 2615–2620.

(55) Ashkenazi, O.; Azulay, D.; Balberg, I.; Kano, S.; Sugimoto, H.; Fujii, M.; Millo, O. Size-Dependent Donor and Acceptor States in Codoped Si Nanocrystals Studied by Scanning Tunneling Spectroscopy. *Nanoscale* **2017**, *9*, 17884–17892.

(56) Tang, J.; Sargent, E. H. Infrared Colloidal Quantum Dots for Photovoltaics: Fundamentals and Recent Progress. *Adv. Mater.* **2011**, *23* (1), 12–29.

(57) Xie, C.; Yan, F. Flexible Photodetectors Based on Novel Functional Materials. *Small* **2017**, *13* (43), 1–36.

(58) Liu, Y.; Gibbs, M.; Puthussery, J.; Gaik, S.; Ihly, R.; Hillhouse, H. W.; Law, M. Dependence of Carrier Mobility on Nanocrystal Size and Ligand Length in Pbse Nanocrystal Solids. *Nano Lett.* **2010**, *10* (5), 1960–1969.

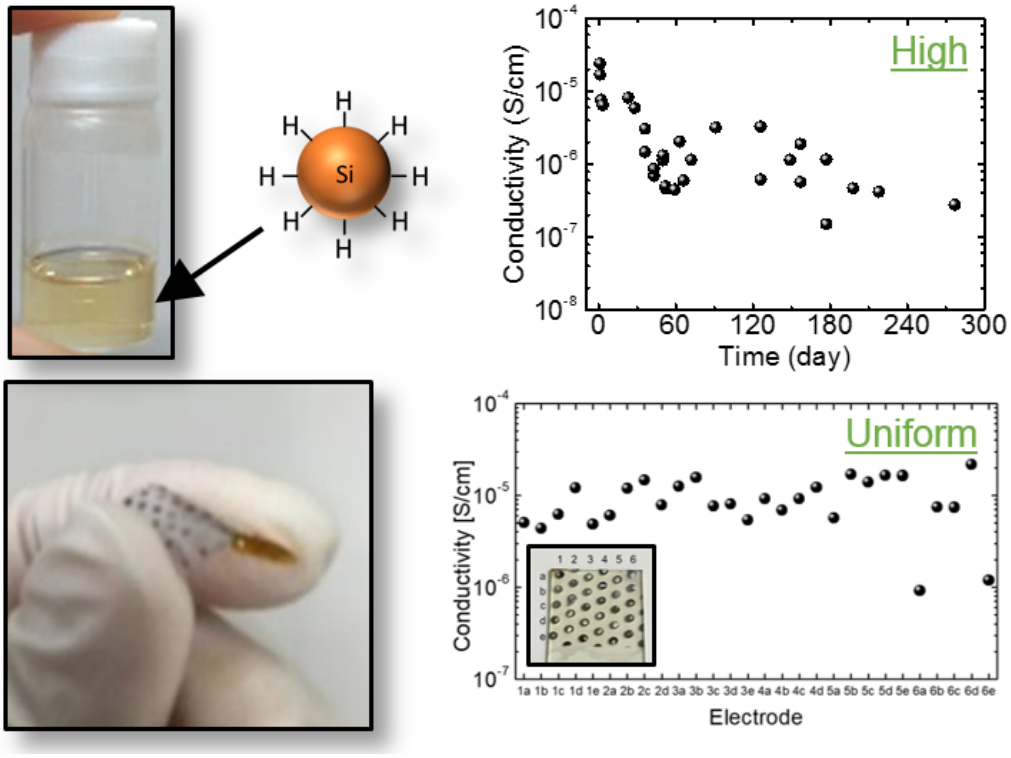

Table of Contents Graphic